NASA

Technical Memorandum 80555

A Spectral Filter for ESMR's Sidelobe Errors

Dennis Chesters

SEPTEMBER 1979

A SPECTRAL FILTER FOR ESMR'S SIDELOBE ERRORS

Dennis Chesters

NASA/Goddard Space Flight Center

Code 915

Greenbelt, Maryland 20771

September 1979

GODDARD SPACE FLIGHT CENTER
Greenbelt, Maryland

Page intentionally left blank

A SPECTRAL FILTER FOR ESMR'S SIDELOBE ERRORS

Dennis Chesters

NASA/Goddard Space Flight Center

Code 915

Greenbelt, Maryland 20771

ABSTRACT

Fourier analysis is used to remove periodic errors from a series of NIMBUS-5 ESMR microwave brightness temperatures. The observations were all taken from the midnight orbits over fixed sties in the Australian grasslands during 1974. The angular dependence of the data indicates calibration errors consisting of broad sidelobes and some miscalibration as a function of beam position. Even though an angular recalibration curve cannot be derived from the available data, the systematic errors can be removed with a spectral filter. The 7-day cycle in the drift of the orbit of NIMBUS-5, coupled to the look-angle biases, produces an error pattern with peaks in its power spectrum at the weekly harmonics. About $\pm 4°K$ of error is removed by simply blocking the variations near two- and three-cycles-per-week.

Page intentionally left blank

CONTENTS

ILLUSTRATIONS

TABLES

Chapter 1

INTRODUCTION

A series of ESMR (Electronically Scanned Microwave Radiometer) brightness temperatures were gathered by Allison et al.,[1] at several sites in the desert and grasslands of eastern Australia, observed from NIMBUS-5 during the first half of 1974. They were studying severe flooding there, using the steady summer data from the grass-covered areas as a baseline. Data was taken from each midnight pass to avoid the diurnal heating cycle. However, the ESMR data were far more variable than the corresponding surface reports. This is the opposite to what would be expected of grass-covered ground, where the vegetation canopy should mask and buffer any changes in the ground's microwave appearance. This study shows how to analyse and correct a sporadically observed series of artificially flickering data without using any other independent observations.

Sporadic problems in the ESMR data-processing chain disqualified one-third of the 120 possible observations at each site. Data from three of the grassland sites is shown in Figure 1, where the few available sequences of consecutive midnight observations are connected by straight lines. The variations shown in Figure 1 are rapid and large, even during the quiet summer months of early 1974. The ESMR data show alternating warm and cold days, correlated among the sites, but not with the local meteorology.

Table 1 lists the cross-correlations between variations in the ESMR temperatures at Cobar and several local meteorological parameters. The modest association of ESMR brightness with air temperature and soil moisture can be accounted for by the general seasonal changes and the autumnal flooding episode. No significant correlation was found between the flicker in the ESMR brightness and local meteorology, even on a delayed basis. Table 1 also lists the mean and standard deviation of each parameter, including the ESMR brightness temperature itself, which has a nominal instrumental noise of $\pm 2°$K.

Table 1
ESMR Brightness at Cobar Correlated with Meteorology

Parameter	Mean ± Standard Deviation	Correlation/ESMR
Air Temperature (°C)	18.4 ± 4.4	+0.58
Dew Point (°C)	13.4 ± 3.6	+0.12
Cloud Cover (Eighths)	3.1 ± 3.1	−0.29
Daily Rainfall (mm)	2.5 ± 8.2	−0.16
Soil Moisture (%)*	44.0 ± 27.0	−0.41
ESMR Brightness Temp. (°K)	258.0 ± 8.0	—

*interpolated from weekly reports

Power spectra were taken of the sporadic series of ESMR temperatures shown in Figure 1. Sharp peaks at 7-day harmonics appeared, which seem related to the weekly drift of NIMBUS-5's orbit in association with regular angle-dependent sidelobe errors.

Rather than doing a complete error analysis of the ESMR data processing chain, we filtered out the obviously artificial periodic variance in the available data, using the data itself as a guide. The purpose of this note is to describe the key ESMR data characteristics and to outline the method for correcting the periodic errors in an irregularly sampled series of observations.

Chapter 2

THE ESMR DATA REDUCTION

Figure 1 shows the ESMR temperatures gathered at three sites: Condobolin, Cobar and Bourke, which are located a few hundred kilometers (a few ESMR beam positions) apart in the arid eastern Australian grasslands, as described by Allison, et al.[1] Because of some unreliability in the map coordinates assigned to the NIMBUS-5 ESMR data, they renavigated each swath by eye to fit the islands and coastlines. When sites fell between nominal ESMR beam-positions, average values of the surrounding pixels were used.

Data was taken within a 120-day period from Australian mid-summer (20 January) to late autumn (19 May) 1974. All three sites experienced severe flooding in autumn (April) 1974, while Bourke also was flooded during summer (February) 1974. This appears as lower ESMR brightness temperatures in Figure 1, due to the low microwave emissivity of water. About 69 of the possible 120 nights have usable ESMR data.

Calibration of the ESMR brightness temperatures was done by the GSFC ERTS/Nimbus Project[2] using their linear recalibration algorithm for each beam position.[3] Their data processing software itself undergoes occasional unpublished revisions.

Figure 1 shows strong correlations in the short period fluctuations of the observed ESMR temperatures among the grassland sites. Table 2 lists the correlations between pairs of sites, before and after filtering of the site observations. Cobar and Condobolin are probably more correlated with each other than with Bourke because they lie close together on similar high, dry grassland, while Bourke is on lightly flooded, stream-fed ground. Indeed, the ESMR observations at Bourke run systematically colder by about 5°K throughout the summer.

The nadir-angle of each observation was estimated by overlaying a Mercator projection of the ESMR beam ground tracks, drawn for Australian latitudes from the nominal orbit description for

Table 2

ESMR Correlations Between Sites
Before/After Filtering

Site/Site	Before	After
Cobar/Bourke	0.58	0.17
Cobar/Condobolin	0.71	0.53
Bourke/Condobolin	0.73	0.22

NIMBUS-5. The angles were estimated by aligning the projection map with the actual swath, to an accuracy of a few degrees of longitude (a few beam positions). Figure 2 shows the ESMR temperatures and corresponding nadir-angles for midnight observations at one site for two months of steady dry summer weather. Note that the orbit is arranged so that if one night's pass looks to the east of nadir, the next night's usually looks to the west. To avoid errors at the edge of the ESMR swaths, observations at nadir angles beyond 40° (out of a possible 50°) were not used.

Figure 3 is a regression plot between these ESMR temperatures and the corresponding nadir angles at all three sites for the quiet summer data. The linear regression lines in Figure 3 indicate a 10°K difference in viewing the same site from the east versus the west. The warmer temperatures recorded when ESMR looked to the east of nadir are interpreted as due to broad sidelobes being filled by the bright Australian continent directly below, as opposed to the cooler temperatures reported when ESMR looked west from over the dark ocean. There are also distinct angle-dependent miscalibrations indicated, with roughly a "skewed W" pattern of being high at the center and edges, and low at 20° from nadir. Figure 3 can show the main features of the inferred nadir-angle dependence of the Australian ESMR temperatures, but it cannot serve as an angular recalibration curve. Fortunately, the data in Figure 1 are good enough to Fourier analyse and correct for nearly all of the periodic errors without additional information.

4

Chapter 3

FOURIER ANALYSIS OF SPORADIC DATA

Although computer oriented formulations of Fourier filtering techniques are now commonly used, the conventions are not yet standardized. Loosely following Brigham,[4] this section casts the basic equations in practical digital form.

The familiar abstract analog form of the Fourier transform pair g(t) and G(f) for time (t) and frequency (f) is shown in Equation (3.1).

$$G(f) = \int_{-\infty}^{\infty} dt \, g(t) \, e^{-2\pi i f t}, \quad g(t) = \int_{-\infty}^{\infty} df \, G(f) \, e^{+2\pi i f t} \tag{3.1}$$

The corresponding indexed series $g\langle k \rangle = g(kT)$ of N discrete measurements, taken at regular time intervals T starting at zero, has a Fourier transform series $G\langle n \rangle = G(n/NT)$, shown in Equation (3.2).

$$G\langle n \rangle = \sum_{k=0}^{N-1} g\langle k \rangle \, e^{-2\pi i k n/N}, \quad g\langle k \rangle = \frac{1}{N} \sum_{n=0}^{N-1} G\langle n \rangle \, e^{+2\pi i k n/N} \tag{3.2}$$

where $\{k\} = \{n\} = \{0, 1, 2, \ldots, N-1\}$.

As usual, the high frequency cutoff was set at the sampling rate 1/T, and the steps in the frequency scale were set equal to the bandwidth resolution limit allowed by the experiment duration rate 1/NT. Equation (3.2) implicitly uses the sampling rate 1/T as the natural rate units. For instance, sampling once per day produces frequency units of cycles per day, so that $n/N = 3/7$ means "three cycles per week." Alternative formulations for Fourier series must be made carefully in order to avoid errors in the normalization and accounting conventions. In particular, the transformation basis exp ($\pm 2\pi i k n/N$) is the only complete orthogonal pair (with a normalization constant equal to N) for the positive indices $\{k\}$ and $\{n\}$. The complex notation for G is actually computed as two parallel series of numbers, the cosine (real) and sine (imaginary) transformation coefficients. Theoretically, N independent complex numbers determine N pairs of transform

coefficients; actually, N real observations reduce the number of independent values in the complex coefficients by imposing the constraint $G\langle n\rangle^* = G\langle N - n\rangle$.

Equation (3.3) defines the low–frequency integrated power P[G] in terms of the power density spectrum $|G|^2$.

$$P\langle n\rangle[G] = \frac{1}{N} \sum_{n'=0}^{n \leq N} |G\langle n'\rangle|^2 \tag{3.3}$$

Note that $|G\langle n\rangle|^2 = |G\langle N - n\rangle|^2$.

Because the norm $|G|^2$ destroys phase information in the power spectrum, it is uniquely determined only for positive frequencies up to one–half of the sampling rate ($n/N \leq 1/2$). The steps in a plot of the integrated power show the fraction of power contained in each resonance peak of the spectrum; the total power is $P\langle N\rangle = \sum |g\langle k\rangle|^2$. In graphical analysis, power is usually shown normalized to the highest peak for spectra, and normalized to the total for accumulated power.

The missing values in a series of measurements are treated as observations of zero weight. Mathematically, a template function g' is created, with value 1 at the time of a good observation, and value 0 at a missing observation. Then, the series of sporadic observations is filled in by using the product $g'g^0$ of the template g' and an ideal series of data g^0. Equation (3.4) shows this construction and the product/convolution theorem for the Fourier transform of such a product of functions.

$$g\langle k\rangle = g'\langle k\rangle g^0\langle k\rangle, \quad G\langle n\rangle = \frac{1}{N} \sum_{n'=0}^{N-1} G'\langle n - n'\rangle G^0\langle n'\rangle \tag{3.4}$$

using $G'\langle -m\rangle = G'\langle m\rangle$ for $\{m\} = \{0,1,2,\ldots,N-1\}$.

Convolution blurs the ideal transform G^0 with the bandpass function G'. Completely regular observations have a strong, sharp bandpass set by the experiment duration rate. While the blur cannot be removed without more information, its power spectrum $|G'|^2$ shows how the pattern of missing observations will broaden or echo the peaks in an ideal spectrum $|G^0|^2$. For instance,

a pattern of regularly missing observations will gene ;te sidelobes from a real peak, due to the frequency ambiguity at the absent cycle rate. A pattern of randomly missing observations merely broadens all features in the power spectrum, due to the absence of some information at all regular sampling rates. The power spectrum of the observation template $|G'|^2$ can be termed the "leakage" in the information spectrum. Basically, some information averaging of less than N independent observations must be done to create N Fourier coefficients.

Sophisticated filters are used when the quality of the data, the nature of the errors, and the data application requirements are all well known. However, with only crude artificial peaks as a guide, the appropriate filter is one that simply blocks all power at the suspected frequency. Because the power spectrum is phase-ambiguous and the filtered result should remain a series of real numbers, the Fourier coefficients must be removed at the conjugate frequency as well (using $G(N-m)=G(m)^*$ for real $g(k)$). Equation (3.5) shows this worked out to produce a new time series $g(k;m)$ with little power at frequency m/N cycles per sample-time, and no variance at the missing observations.

$$g(k;m) = g'(k)\left\{g(k) - (2/N)[\,Re(G(m))\cos(2\pi km/N) - Im(G(m))\sin(2\pi km/N)]\right\} \quad (3.5)$$

for frequency $0 < m/N < 1/2$.

The filter imposed by Euqation (3.5) first removes all variations at the suspected frequency. This creates fluctuations in the regularized series of filtered observations at the times when no observation was taken. When the observation template g' is used to suppress the induced fluctuations, the cleanly blocked power spectrum is again blurred according to the product/convolution theorem of Equation (3.4). The effect is to level the final filtered spectrum a little, by spreading the available information over all N spectral points. If more than one frequency is to be blocked, all of the corresponding Fourier coefficients should be subtracted in Equation (3.5) before being multiplied by the template g'. The blocking filter of Equation (3.5) removes all variations at the

suspected frequency, including the natural ones. This loss amounts to only 2/N of the total natural variance, for a well-sampled series with a naturally flat power spectrum.

The following steps outline the algorithm for removing most of the simple periodic errors in a series of data with missing observations:

1. Select a sequence of observations that should be internally consistent.

2. Subtract the average value to make a series of sporadic variations g^0, and create an observation template g'.

3. Create the regularly sampled series $g = g'g^0$ by setting the unobserved variations to zero value.

4. Calculate and plot the normalized power spectra $|G'|^2$ and $|G|^2$ to see how the missing observations might distort the resonant peaks.

5. Classify peaks as "artificial" if they are strong, are unrelated to natural physical causes, are unrelated to bandpass function distoritons of other peaks, and/or are near suspicious harmonics.

6. Remove the "artificial" periodicities with Equation (3.5) to form a filtered sporadic series $g(k;m,m',\ldots)$.

7. Compare the integrated power $P[G]$ before and after filtering, and estimate the amount of erroneous variance removed.

8. Add the original mean value back to the filtered series for subsequent scientific analysis.

Chapter 4

FILTERING THE ESMR DATA

We will step through the filtering algorithm for the 1974 summer Cobar series of ESMR brightness temperatures shown in Figure 2, and then tabulate the effect of similar filters for the other cases shown in Figure 1.

Power spectra $|G|^2$ and the corresponding bandpass function $|G'|^2$ of the uniformly resampled ESMR variations from Figure 2 are shown in Figure 4. Even though there are only 41 good observations in 62 days, the bandpass $|G'|^2$ is well behaved, with only minor sidebands at 1/7 and 3/7 (once and thrice per week) due to some regularity in the missing observations (no Saturdays). However, the ESMR variations themselves show strong artificial peaks near frequencies of 2/7 and 3/7, and a natural low-frequency drift. The association of the artificial ESMR temperature periodicities with angular biases is strengthened by the similarity between their power spectra (compare Figures 4 and 5).

Figure 6 shows that one-third of the total variance in the ESMR temperatures is removed by applying blocking filters near the artificial frequencies 2/7 and 3/7 (actually at $m/N = 17/62$ and 26/62). Specifically, the standard deviation of the sporadic series decreased from $\pm 5.5°K$ to $\pm 4.3°K$, removing $\pm 3.4°K$. Comparison of Figures 3 and 7 shows that most of the inferred correlation between ESMR temperature and scan angle is removed by the blockage of the weekly periodicities.

Table 3 lists the improvements in the standard deviations of the ESMR temperatures at all three grassland sites in summer and autumn. The residuals after filtering are white noise and long period drifts, in about equal amounts. The seasons are handled separately not only because of the climatic differences, but also because of the large gap in the ESMR observations at the change of seasons. Note that an orbital change would require the start of a new filter, because a phase-shift induced by the change would violate the simple periodicity assumed in the blocking filter.

Table 3
ESMR Standard Deviations Before/After Filtering

Season	Site	Before	After	Removed
summer	Cobar	±5.5°K	±4.3°K	±3.4°K
summer	Condobolin	±6.0°K	±3.6°K	±4.8°K
summer	Bourke	±6.7°K	±5.5°K	±3.8°K
autumn	Cobar	±6.7°K	±5.1°K	±4.4°K
autumn	Condobolin	±7.1°K	±5.6°K	±4.4°K
autumn	Bourke	±6.6°K	±5.3°K	±3.9°K

Finally, comparison of Figures 8 and 1 shows the improvement in all series of ESMR temperatures when the weekly harmonics are blocked. For each of these cases, the periodic errors added about ±4°K, due mainly to the large east-west bias from the bright Australian continent filling broad sidelobes in the ESMR antenna pattern. Note that the flooding episode in the autumnal observations is actually clarified by the filtering, which was, after all, the original purpose in devising a correction scheme for Allison's[1] 1974 Australian ESMR data.

Chapter 5

COMMENTS ON ESMR DATA

Many of the missing ESMR observations were rejected because the data swaths showed "glitch mode" patterns—streaks of artificially high or low brightness running parallel to the satellite ground track. In fact, the gap in the Australian ESMR data in April 1974 was due to a continuous "glitch mode" episode. It seems likely that the low temperatures frequently recorded at 20° to either side of nadir are a subtler form of this.

The observations which were taken at the Australian desert sites from the same ESMR swaths were too few and too biased toward the swath's edge for good filter analysis. They did show considerably more variance, with crude periodic errors having weekly harmonics and angle-dependence.

The Australian ESMR data were reduced in ways aimed to avoid the foreseeable errors. The normal diurnal variations in ground temperature were minimized in the ESMR temperatures by the use of only midnight observations. Faulty geographic positioning of the ESMR data was corrected by the renavigation of each image with the coastline of eastern Australia. Variations due to the details of the local geography should be minimized by the fact that the sites are located in a homogeneous area. The use of grassland sites, whose microwave appearance is buffered by the vegetation, and the lack of correlation with local meteorology indicates that the periodic errors are essentially instrumental.

Current users of NIMBUS-5 ESMR data do not find problems of exactly our type, but they do not work with months of ESMR data on a bright continent that fills much of the potential sidelobes. For instance, Kidder[5] corrected calibration insensitivity at beam positions near small and large nadir angles by requiring steady averages from the quiet open tropical ocean. Likewise, Carsey[6] rejects data containing significant dips in running-mean values of the ESMR brightness of the open Antarctic Ocean. Without undertaking a major project to analyse ESMR errors, we

11

are unable to prove whether or not the periodic (nadir-angle) errors are really unique to the 1974 Australian data, or are merely enhanced by the unusual use of it.

Future users of ESMR data should be supplied with a technical summary of the antenna pattern, of known problems, and of the results of verification experiments. If another ESMR is ever launched, a thorough pre-launch calibration of the antenna pattern for each beam position is needed to understand for the sidelobes. Otherwise, good quantitative work near the bright/dark land/sea boundaries is impossible.

APPENDIX A

FIGURES USED
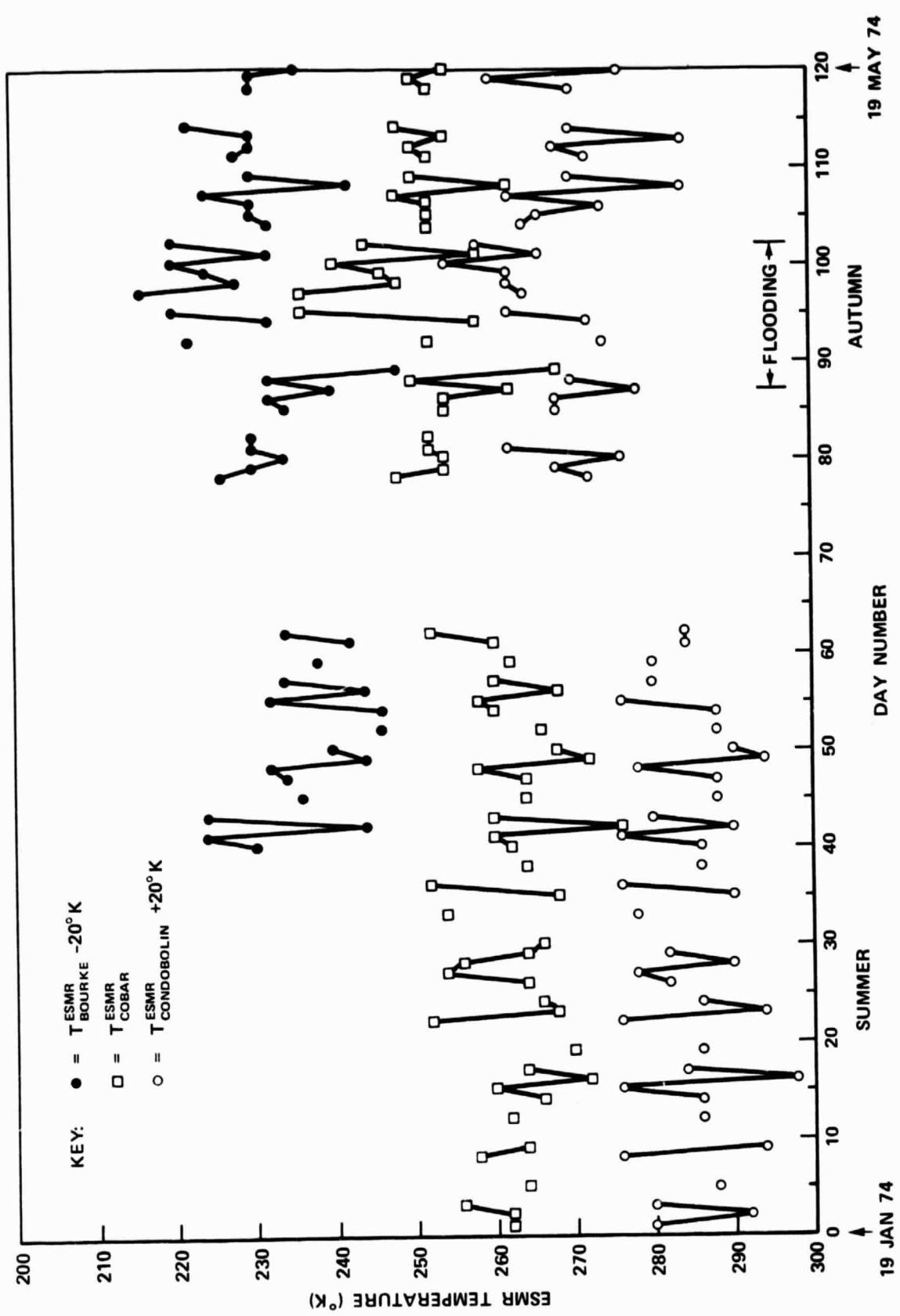
Figure 1. Midnight ESMR Brightness Temperatures at Three Sites

13
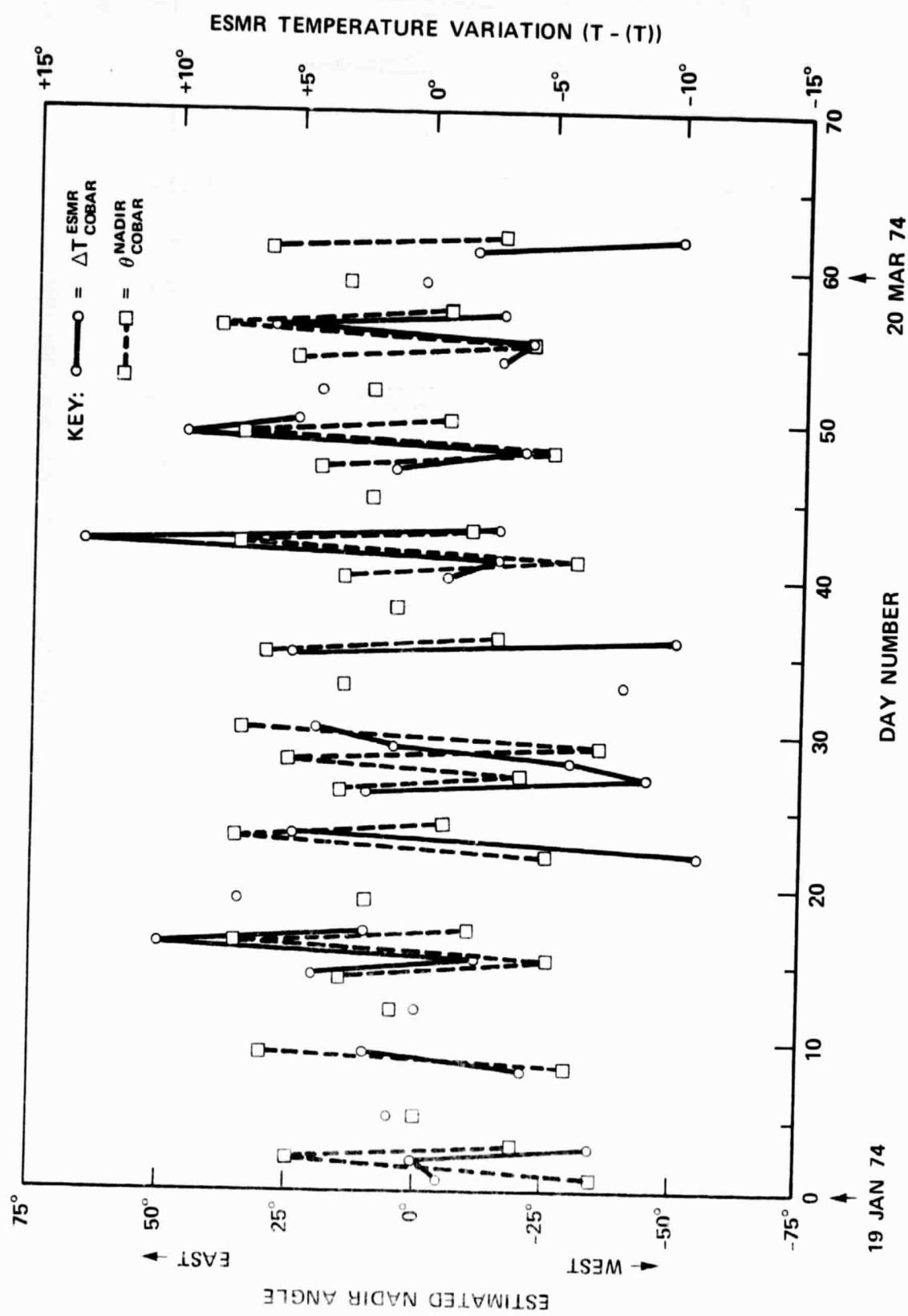
Figure 2. Summer ESMR Temperature and Nadir–Angle at Cobar
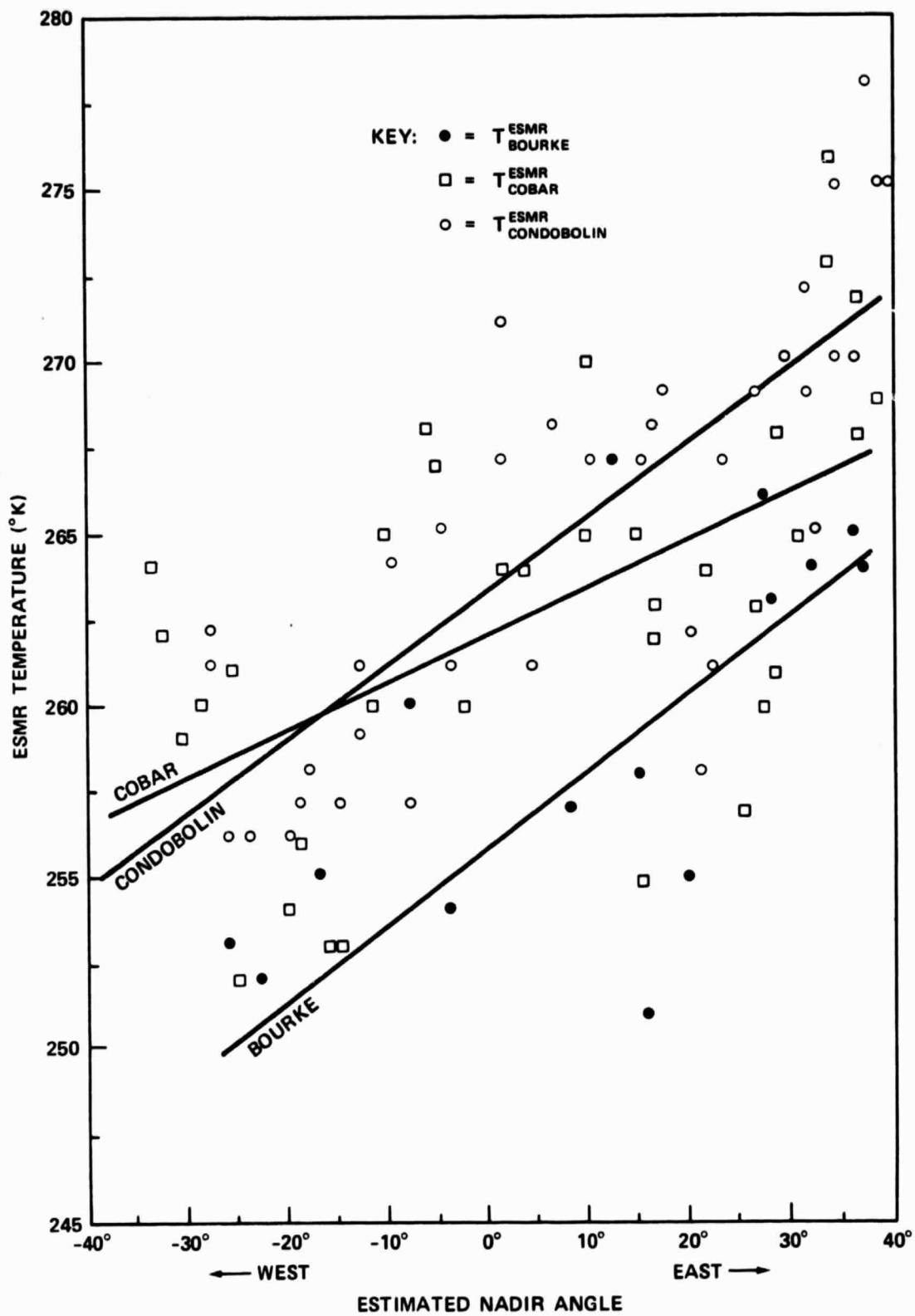
Figure 3. Summer ESMR Temperature vs. Nadir-Angle at Three Sites
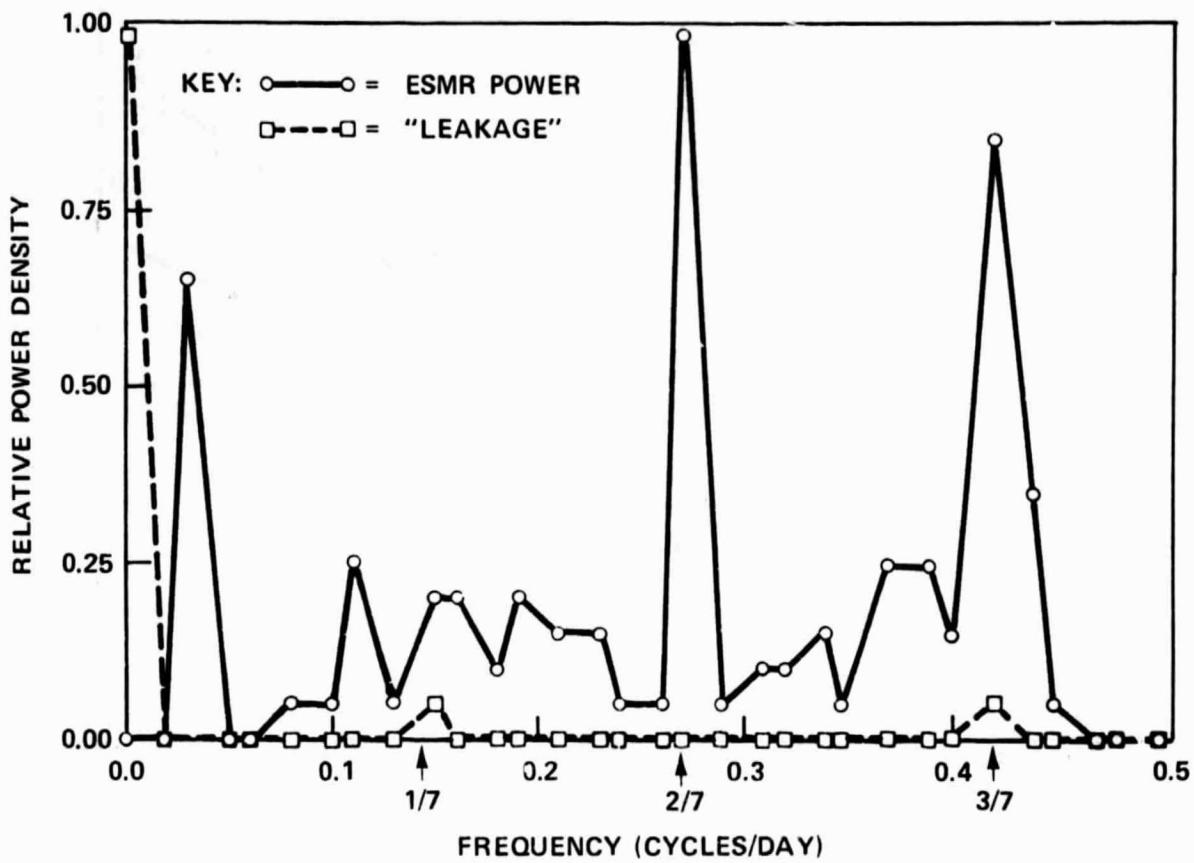
Figure 4. Power Spectrum of Summer Cobar ESMR Variations
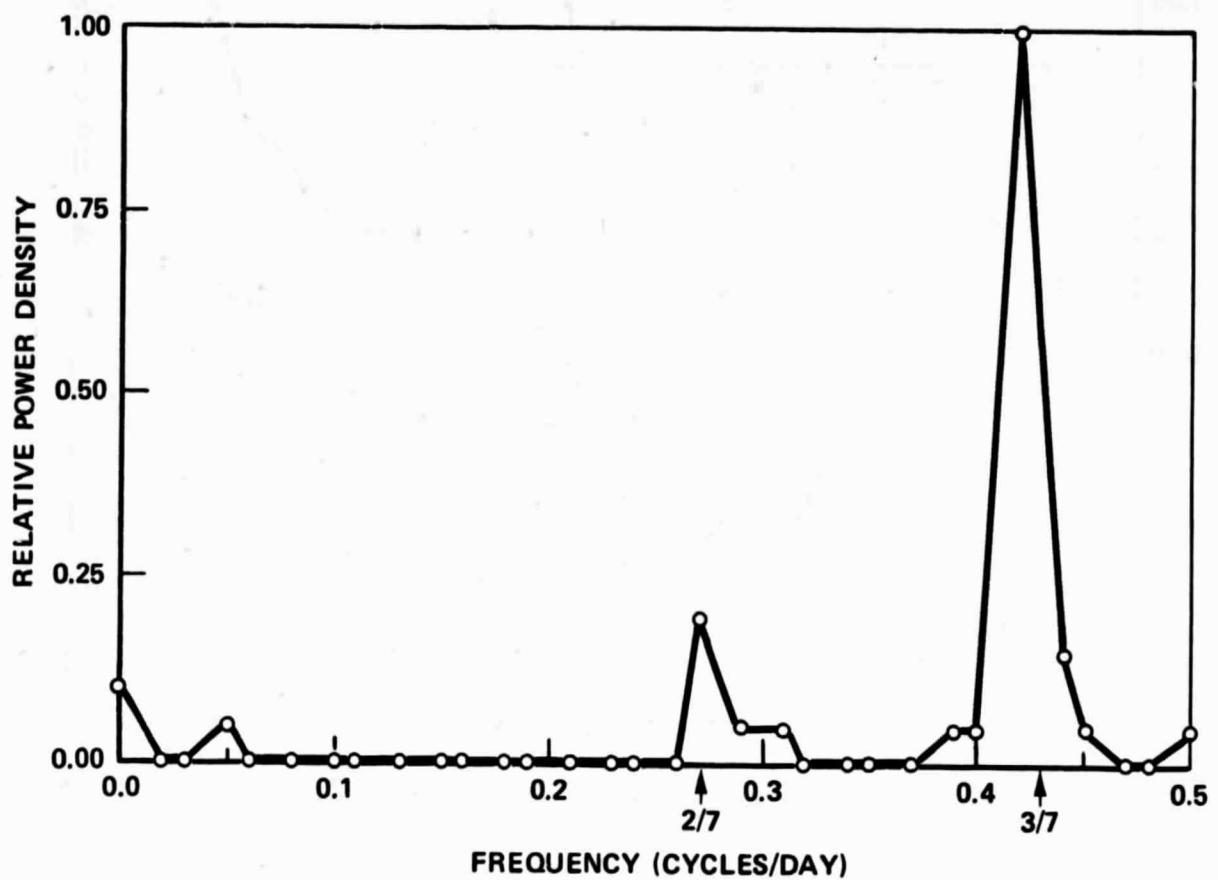
Figure 5. Power Spectrum of Summer Cobar Nadir Angles

17
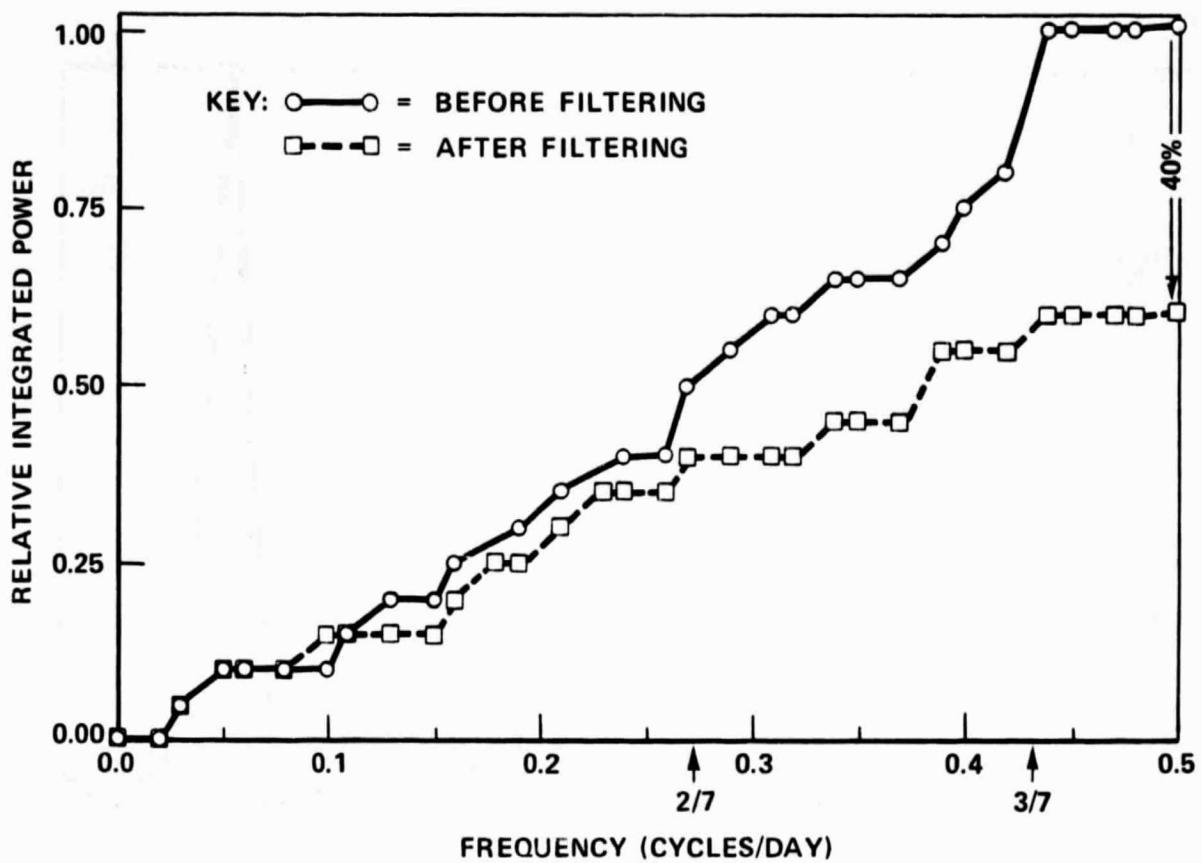
Figure 6. Integrated Power for Summer Cobar Before/After Filtering
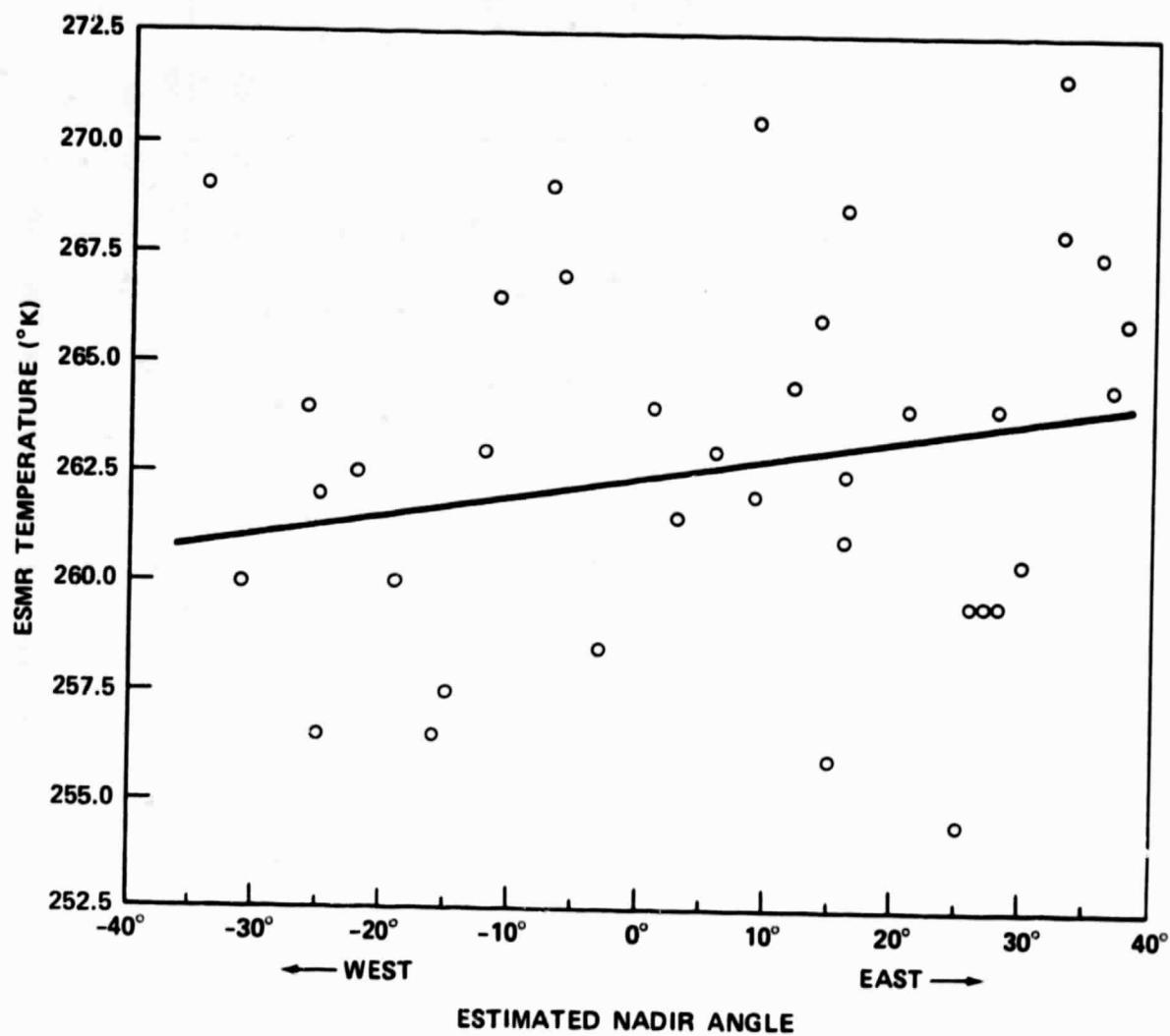
Figure 7. Filtered ESMR Temperatures vs. Nadir–Angle at Cobar

19
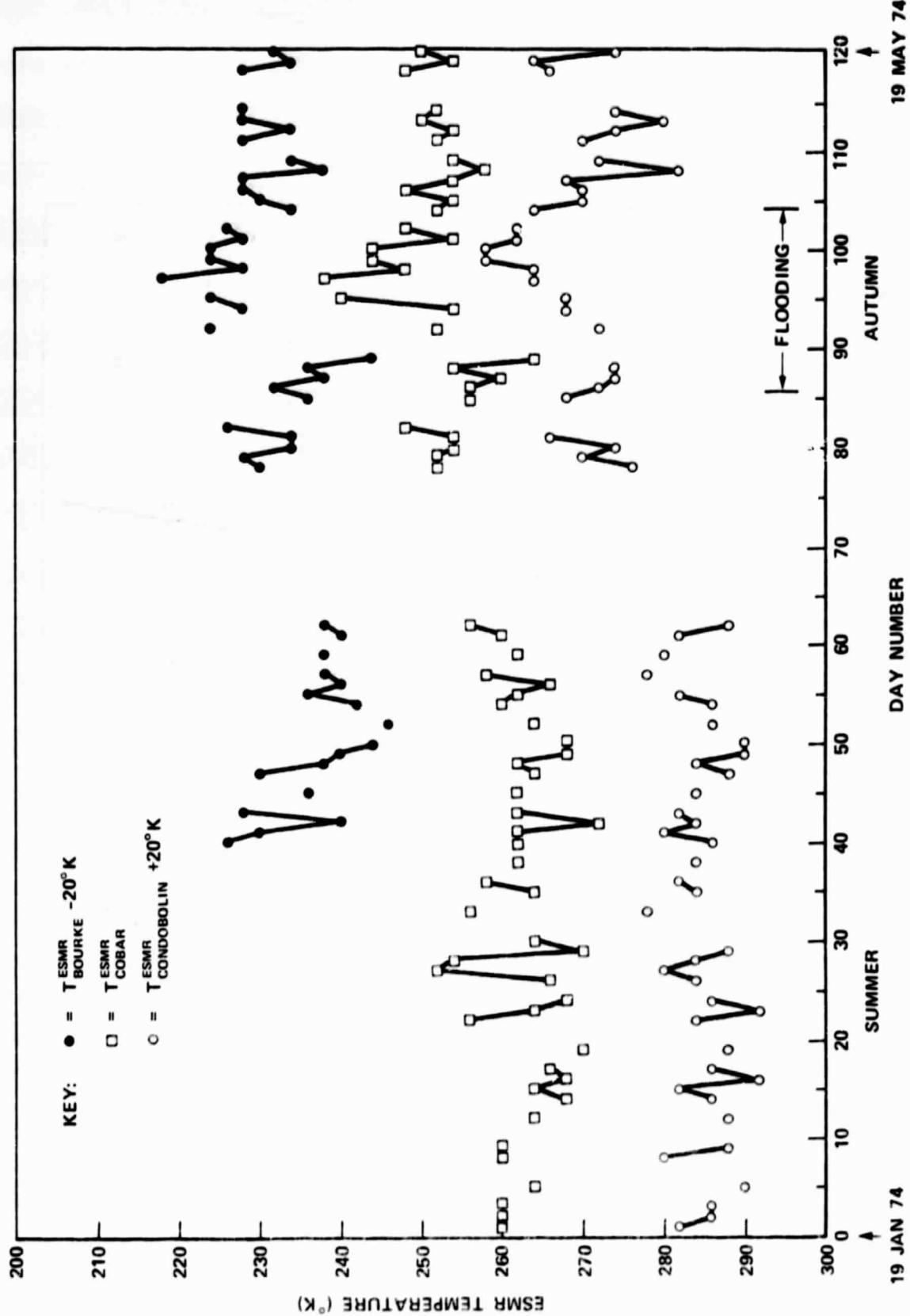
Figure 8. Filtered Series of ESMR Temperatures at Three Sites

20

REFERENCES

1. Allison, L. J., Schmugge, T. J., and Byrne, G., A Hydrological Analysis of East Australian Floods Using Nimbus-5 Electrically Scanning Microwave Radiometer Data, NASA/GSFC TM 79689, March 1979.

2. Wilheit, T., "The Electrically Scanning Microwave Radiometer (ESMR) Experiment," The NIMBUS-5 User's Guide, NASA/GSFC, 1972.

3. The NIMBUS-5 Data Catalog, Volume 2, NASA/GSFC, Section 5-3, "ESMR Corrections to the User's Guide (New)," pp. 5-4 to 5-6, 1973.

4. Brigham, E. O., The Fast Fourier Transform, Prentice-Hall, 1974.

5. Kidder, S. O. and Vonder Haar, T. H., Seasonal Oceanic Precipitation Frequencies from Nimbus-5 Microwave Data, JGR, Vol. 82, pp. 2083-2086.

6. Carsey, F., NASA/GSFC, private communication, 1979.

BIBLIOGRAPHIC DATA SHEET

1. Report No. TM 80555	2. Government Accession No.	3. Recipient's Catalog No.
4. Title and Subtitle A SPECTRAL FILTER FOR ESMR'S SIDELOBE ERRORS		5. Report Date September, 1979
		6. Performing Organization Code 915
7. Author(s) Dennis Chesters		8. Performing Organization Report No.
9. Performing Organization Name and Address Goddard Space Flight Center Greenbelt, MD 20771		10. Work Unit No.
		11. Contract or Grant No.
		13. Type of Report and Period Covered Reference Publication
12. Sponsoring Agency Name and Address National Aeronautics and Space Administration Washington, D.C. 20546		
		14. Sponsoring Agency Code A-12

15. Supplementary Notes

16. Abstract

Fourier analysis is used to remove periodic errors from a series of NIMBUS-5 ESMR microwave brightness temperatures. The observations were all taken from the midnight orbits over fixed sties in the Australian grasslands during 1974. The angular dependence of the data indicates calibration errors consisting of broad sidelobes and some miscalibration as a function of beam position. Even through an angular recalibration curve cannot be derived from the available data, the systematic errors can be removed with a spectral filter. The 7-day cycle in the drift of the orbit of NIMBUS-5, coupled to the look-angle biases, produces an error pattern with peaks in its power spectrum at the weekly harmonics. About $\pm 4°K$ of error is removed by simply blocking the variations near two- and three-cycles-per-week.

17. Key Words (Selected by Author(s)) Microwave, Sidelobe, Calibration	18. Distribution Statement Unclassified-Unlimiter Star 88 Space Sciences

19. Security Classif. (of this report) Unclassified	20. Security Classif. (of this page) Unclassified	21. No. of Pages 21	22. Price*